

## **SIMULATION OF ELECTROMAGNETIC DIFFUSION IN ANISOTROPIC MEDIA**

**J. M. Carcione**

Istituto Nazionale di Oceanografia e di Geofisica Sperimentale (OGS)  
Borgo Grotta Gigante 42c, Sgonico 34010, Trieste, Italy

**Abstract**—I present an algorithm to simulate low-frequency electromagnetic propagation in an anisotropic earth, described by a general (non-diagonal) conductivity tensor. I solve the electric formulation by explicitly imposing an approximate form of the condition  $\nabla \cdot \mathbf{J} = 0$ , where  $\mathbf{J}$  is the current density vector, which includes the source and the induced current. The numerical algorithm consists of a fully spectral explicit scheme for solving linear, periodic parabolic equations. It is based on a Chebyshev expansion of the evolution operator and the Fourier and Chebyshev pseudospectral methods to compute the spatial derivatives. The latter is used to implement the air/ocean boundary conditions. The results of the simulations are verified by comparison to analytical solutions obtained from the Green function. Examples of the electromagnetic field generated by a source located at the bottom of the ocean illustrate the practical uses of the algorithm.

### **1. INTRODUCTION**

Electromagnetic modeling and propagation at low frequencies (electromagnetic diffusion) is used in a number of applications, such as geothermal exploration [26], evaluation of hydrocarbon resources by mapping the sub-seafloor resistivity [14], electromagnetic induction in boreholes and logging while drilling [33], magnetotelluric problems [21, 37], and geoelectrical surveys for groundwater and mineral exploration [25].

Most of the numerical algorithms are based on low-order finite-differences (FD) to compute the spatial derivatives. Many authors use the classical FD methods, with different approaches to recast the

electromagnetic equations, in the time or frequency domains. For instance, Lee et al. [18] propose to transform the 3-D diffusion equation into a wave equation by introducing a new variable proportional to the square root of time. Leppin [19] solved the 2.5-D transient electromagnetic scattering problem, where the governing diffusion equation has been formulated in terms of the magnetic field, and through the introduction of an exact boundary condition at the air-earth interface.

Wang and Hohmann [32] generalized the 2-D algorithm of Oristaglio and Hohmann [25] to three dimensions. They developed a magnetic/electric formulation of Maxwell's equations, using as a solver a staggered grid and a modified version of the Du Fort-Frankel method. The use of an artificially high permittivity allows them to reduce the computer time. A 3-D solution based on a linear-system frequency-domain formulation of the diffusion equation has been proposed by Weiss and Newman [35]. Their work on preconditioning closely follows that of Druskin and Knizhnerman [12] and, particularly, Druskin et al. [13], which resulted in a factor of 100 speed-up of the spectral Lanczos decomposition method.

Badea et al. [5] developed a 3-D finite-element method to solve controlled-source electromagnetic (EM) induction problems in heterogeneous electrically conducting media. The solution is based on a weak formulation of the governing Maxwell equations using Coulomb-gauged electromagnetic potentials. The divergence-free condition  $\nabla \cdot \mathbf{J} = 0$  is imposed, corresponding to inductively coupled sources.

Weiss and Constable [34] developed a 3-D Cartesian finite-volume solution to the time-harmonic (frequency-domain) Maxwell equations. Maaø [20] performed 3-D simulations with a FD method by using a mathematical transformation similar to the Kelvin-Voigt viscoelastic model. This model introduces a high permittivity as in the case of Wang and Hohmann [32]. Maaø [20] further reduced the computer time solving the equations in the high-frequency range by using a complex-frequency Fourier transform to filter high-frequency wave-like signals.

There are many material configurations in the subsurface that might lead to anisotropy [23]. The geophysical motivation behind the use of an electrically anisotropic description of the Earth can be found in many works [4, 6, 9, 31, 35, 38]. It might be that there are some preferred directions in the subsurface rocks, or some preferred orientation of grains in the sediments. Compaction, fine layering or a pronounced strike direction might lead to effective anisotropy. Alternations of sandstone and shales may give reservoir anisotropy [8, 11]. Anisotropy can lead to misleading interpretations. For instance, Everett and Constable [15] note a paradox of electrical

anisotropy, by which there is higher apparent conductivity across the strike of anisotropy, which is opposite of what actually exists. Al-Garni and Everett [3] resolve the paradox by recognizing that the response is actually controlled by the conductivity in the direction of the local-induced current flow beneath the receiver loop.

Several algorithms have been developed for electromagnetic logging in wells assuming material anisotropy, for instance, Wang and Fang [31] and Weiss and Newman [35] developed classical FD methods for this purpose, and Davydycheva et al. [11] use a FD Lebedeva staggered grid. Kong et al. [17] developed a 2.5-D finite-element modeling method for marine controlled-source electromagnetic (CSEM) applications in stratified anisotropic media with a diagonal conductivity tensor. Since the implementation of sources in electromagnetic diffusion generates noise, the total field is obtained as the sum of the analytical background field calculated with a 1-D modeling method and the scattered field obtained by using delta sources with and without target.

Carcione [7,8] proposed an spectral algorithm to solve for electromagnetic diffusion in 2-D isotropic media. The algorithm uses an explicit scheme based on a Chebyshev expansion of the evolution operator in the domain of the eigenvalues of the propagation matrix [30]. The spatial derivatives are computed with the Fourier pseudospectral method, which allows the use of coarser grids compared to FD methods. The modeling allows general material variability, a non-diagonal conductivity tensor and provides snapshots and time histories of the electric and magnetic fields. The use of this spectral method overcomes two drawbacks: low accuracy and stringent stability conditions, since the error in time decays exponentially. This algorithm is generalized to the 3-D case and the air/ocean boundary conditions is implemented to deal with CSEM applications.

The performance of the algorithm is verified by comparison to analytical solutions for anisotropic homogeneous media. Finally, examples in inhomogeneous media illustrates a practical application.

## 2. MAXWELL'S EQUATIONS FOR GENERAL ANISOTROPIC MEDIA

In 3-D vector notation, Maxwell's equations, neglecting the displacement currents, are [8]:

$$\begin{aligned}\nabla \times \mathbf{E} &= -\partial_t \mathbf{B}, \\ \nabla \times \mathbf{H} &= \mathbf{J}_I + \mathbf{J}_S \equiv \mathbf{J},\end{aligned}\tag{1}$$

where the vectors  $\mathbf{E}$ ,  $\mathbf{H}$ ,  $\mathbf{B}$ ,  $\mathbf{J}_I$  and  $\mathbf{J}_S$  are the electric field intensity, the magnetic field intensity, the magnetic flux density, the induced current

density, and the electric source current, respectively. In general, they depend on the Cartesian coordinates  $(x_1, x_2, x_3) = (x, y, z)$ , and the time variable  $t$ . The compact notation  $\partial_t \equiv \partial/\partial t$  is used.

Additional constitutive equations are needed. These are  $\mathbf{J}_I = \boldsymbol{\sigma} \cdot \mathbf{E}$  and  $\mathbf{B} = \mu \mathbf{H}$ , where  $\boldsymbol{\sigma}$ , the conductivity tensor, is a real, symmetric and positive definite tensor, and  $\mu$ , the magnetic permeability, is a scalar quantity, and the dot denotes ordinary matrix multiplication.

Substituting the constitutive equations into Equations (1) gives

$$\begin{aligned} \nabla \times \mathbf{E} &= -\mu \partial_t \mathbf{H}, \\ \nabla \times \mathbf{H} &= \boldsymbol{\sigma} \cdot \mathbf{E} + \mathbf{J}_S, \end{aligned} \quad (2)$$

which are a system of six scalar equations in six scalar unknowns.

In this work, I am concerned with triclinic media, where at each point of the space the conductivity tensor is of the form

$$\boldsymbol{\sigma} = \begin{pmatrix} \sigma_{11} & \sigma_{12} & \sigma_{13} \\ \sigma_{12} & \sigma_{22} & \sigma_{23} \\ \sigma_{13} & \sigma_{23} & \sigma_{33} \end{pmatrix}. \quad (3)$$

For a given homogeneous medium, the tensor can always be rotated to obtain its expression in its principal coordinate system:

$$\boldsymbol{\sigma} = \begin{pmatrix} \sigma_1 & 0 & 0 \\ 0 & \sigma_2 & 0 \\ 0 & 0 & \sigma_3 \end{pmatrix}. \quad (4)$$

Without loss in generality, this form can be used to study the physics of the diffusion process, but the numerical solutions are obtained with the expression (3).

Although the magnetic permeability is commonly assumed to be that of free space, some soils have a significantly higher value [24], hence,  $\mu$  can vary arbitrarily in space. In some cases, such as the CSEM problems  $\mu$  is assumed to be spatially constant.

### 3. ELECTRIC FORMULATION

From Equation (1) I obtain a vector equation for the electric field:

$$-\partial_t \mathbf{E} = \boldsymbol{\sigma}^{-1} \cdot [\nabla \times (\mu^{-1} \nabla \times \mathbf{E}) + \partial_t \mathbf{J}_S]. \quad (5)$$

Note that

$$\nabla \times (\mu^{-1} \nabla \times) = \begin{pmatrix} -(\partial_2 \mu^{-1} \partial_2 + \partial_3 \mu^{-1} \partial_3) & \partial_2 \mu^{-1} \partial_1 & \partial_3 \mu^{-1} \partial_1 \\ \partial_1 \mu^{-1} \partial_2 & -(\partial_1 \mu^{-1} \partial_1 + \partial_3 \mu^{-1} \partial_3) & \partial_3 \mu^{-1} \partial_2 \\ \partial_1 \mu^{-1} \partial_3 & \partial_2 \mu^{-1} \partial_3 & -(\partial_1 \mu^{-1} \partial_1 + \partial_2 \mu^{-1} \partial_2) \end{pmatrix}, \quad (6)$$

where I have denoted  $\partial/\partial x_i$  by  $\partial_i$  for brevity. Equation (5) can be solved for  $\mathbf{E} = (E_1, E_2, E_3)^\top$ .

Following Badea et al. [5] and Stalnaker [29], I consider the case

$$\nabla \cdot \mathbf{J} = \nabla \cdot (\boldsymbol{\sigma} \cdot \mathbf{E}) = 0, \tag{7}$$

which is valid for  $\nabla \cdot \mathbf{J}_S = 0$ , according to Equation (1), i.e., if the source current density is divergence-free. This condition is satisfied by inductively coupled magnetic dipole controlled sources of the form

$$\mathbf{J}_S = \nabla \times \mathbf{A}, \tag{8}$$

where  $\mathbf{A}$  is a vector. In the 2-D plane-wave case discussed later (propagation in the  $(x, z)$ -space), an example is  $\mathbf{A} = (0, fh, 0)^\top$ , and  $\mathbf{J}_S = (-\partial_3 f, \partial_1 f)^\top h$ , where  $f(\mathbf{x})$  is the spatial distribution and  $h(t)$  is the time history.

Condition (7) has to be imposed according to the approach illustrated in the next sections. The numerical algorithm presented here is not restricted to divergence-free sources. Also, non divergence-free electric dipole sources can be implemented, but Equation (7) has to be modified accordingly. However, as illustrated in the examples, the divergence-free property is not preserved by the partial differential equations and condition (7) is required when using divergence-free sources. The general question of the computation of the divergence-free part of a vector field arises in many problems of physical interest, for example, in electromagnetism [16] and in the Navier-Stokes equations for incompressible fluids. Specifically, the divergence-free condition addressed here has been considered by Smith [28] and Sasaki and Meju [27].

### 3.1. Homogeneous Media

I consider in this section a version of the differential equations for a homogeneous anisotropic medium. The purpose is to test the Chebyshev algorithm for time integration using the electric formulation. For simplicity and without loss of generality, the conductivity tensor is considered in its principal system. The tensor is diagonal and I denote  $\sigma_i = \sigma_{i(i)}$ . From Equation (7), I have

$$\sigma_1 \partial_1 E_1 + \sigma_2 \partial_2 E_2 + \sigma_3 \partial_3 E_3 = 0. \tag{9}$$

Note that in homogeneous anisotropic media  $\nabla \cdot \mathbf{E} \neq 0$ , while in homogenous isotropic media  $\nabla \cdot \mathbf{E} = 0$ . When the medium is inhomogeneous this condition is not valid in any case.

Equation (5) becomes

$$-\partial_t \mathbf{E} = \boldsymbol{\gamma} \cdot \nabla \times \nabla \times \mathbf{E}, \tag{10}$$

where

$$\gamma = (\mu\sigma)^{-1}. \quad (11)$$

I have assumed that the magnetic permeability is a constant, as is the case in many geophysical applications. The explicit form of Equation (10) is

$$\begin{aligned} -\partial_t E_1 &= \gamma_1 [ -(\partial_2^2 E_1 + \partial_3^2 E_1) + \partial_2 \partial_1 E_2 + \partial_3 \partial_1 E_3 ], \\ -\partial_t E_2 &= \gamma_2 [ -(\partial_1^2 E_2 + \partial_3^2 E_2) + \partial_2 \partial_1 E_1 + \partial_3 \partial_2 E_3 ], \\ -\partial_t E_3 &= \gamma_3 [ -(\partial_1^2 E_3 + \partial_2^2 E_3) + \partial_1 \partial_3 E_1 + \partial_2 \partial_3 E_2 ]. \end{aligned} \quad (12)$$

If the medium is isotropic (and homogeneous), I can use the property  $\nabla \times \nabla \times \mathbf{E} = \nabla(\nabla \cdot \mathbf{E}) - \nabla^2 \mathbf{E} = -\nabla^2 \mathbf{E}$ . Then, Equation (5) becomes

$$\partial_t \mathbf{E} = \gamma \nabla^2 \mathbf{E}, \quad \gamma = \frac{1}{\mu\sigma}, \quad (13)$$

where

$$\nabla^2 \mathbf{E} = (\nabla^2 E_1, \nabla^2 E_2, \nabla^2 E_3)^\top. \quad (14)$$

Next, I consider the 2-D anisotropic case, by assuming an infinite plane-wave along the  $y$ -direction. The  $y$ -derivates vanish and the  $E_2$  and  $(E_1, E_3)$  fields decouple. The equations, corresponding to the coupled components, are

$$\begin{aligned} -\partial_t E_1 &= \gamma_1 (-\partial_3^2 E_1 + \partial_3 \partial_1 E_3), \\ -\partial_t E_3 &= \gamma_3 (-\partial_1^2 E_3 + \partial_1 \partial_3 E_1). \end{aligned} \quad (15)$$

Because  $\text{div} \cdot \mathbf{J}_I = 0$  one has  $\sigma_1 \partial_1 E_1 + \sigma_3 \partial_3 E_3 = 0$ . Combining this equation with (15) yields

$$\begin{aligned} \partial_t E_1 &= \gamma_1 \partial_3^2 E_1 + \gamma_3 \partial_1^2 E_1 = \Delta_\gamma E_1, \\ \partial_t E_3 &= \gamma_3 \partial_1^2 E_3 + \gamma_1 \partial_3^2 E_3 = \Delta_\gamma E_3, \end{aligned} \quad (16)$$

where

$$\Delta_\gamma = \gamma_1 \partial_3^2 + \gamma_3 \partial_1^2 = \frac{1}{\mu\sigma_3} \partial_1^2 + \frac{1}{\mu\sigma_1} \partial_3^2 \quad (17)$$

is a modified Laplacian. Note that the field components have decoupled. The 2-D analytical solution is given in Appendix A.

In 3-D space, the  $E_3$ -component can be decoupled if one considers a transversely isotropic medium with  $\sigma_1 = \sigma_2$ . In this case, a similar procedure leads to

$$\partial_t E_3 = \Delta_\gamma E_3, \quad (18)$$

where

$$\Delta_\gamma = \gamma_1 \partial_3^2 + \gamma_3 (\partial_1^2 + \partial_2^2), \quad (19)$$

and a corresponding analytical solution can easily be obtained.

### 3.2. Inhomogeneous Media

In the inhomogeneous case, the non-diagonal conductivity tensor has to be used, since the properties of the medium can vary arbitrarily. Then, Equation (6) is considered, although for geophysical applications  $\mu$  can be assumed constant as stated above. To obtain a 2-D version of (5), I assume that the properties along the  $y$ -direction are constant. Disregarding the sources for simplicity, I obtain

$$\begin{aligned} -\partial_t E_1 &= \gamma_{11}(-\partial_3^2 E_1 + \partial_1 \partial_3 E_3) - \gamma_{12}(\partial_1^2 + \partial_3^2)E_2 + \gamma_{13}(-\partial_1^2 E_3 + \partial_1 \partial_3 E_1), \\ -\partial_t E_2 &= \gamma_{12}(-\partial_3^2 E_1 + \partial_1 \partial_3 E_3) - \gamma_{22}(\partial_1^2 + \partial_3^2)E_2 + \gamma_{23}(-\partial_1^2 E_3 + \partial_1 \partial_3 E_1), \\ -\partial_t E_3 &= \gamma_{13}(-\partial_3^2 E_1 + \partial_1 \partial_3 E_3) - \gamma_{23}(\partial_1^2 + \partial_3^2)E_2 + \gamma_{33}(-\partial_1^2 E_3 + \partial_1 \partial_3 E_1), \end{aligned} \tag{20}$$

where  $\gamma_{ij}$  are the components of  $(\mu\sigma)^{-1}$  given in Equation (11). The components  $E_2$ ,  $H_1$  and  $H_3$  are decoupled from  $H_2$ ,  $E_1$  and  $E_3$  only if the conductivity tensor is diagonal. In this case, a version of the isotropic diffusion equation is obtained, where the only conductivity involved in the equation is  $\sigma_{22}$  and the field component is  $E_2$ . This is the TE equation solved by Oristaglio and Hohmann [25], while  $E_1$  and  $E_3$  are coupled and satisfy the TM equation.

Alternatively, one may arbitrarily ignore the  $y$ -dimension and obtain equations for a 2-D world when the conductivity tensor is not diagonal,

$$\begin{aligned} -\partial_t E_1 &= \gamma_{11}(-\partial_3^2 E_1 + \partial_1 \partial_3 E_3) + \gamma_{13}(-\partial_1^2 E_3 + \partial_1 \partial_3 E_1), \\ -\partial_t E_3 &= \gamma_{13}(-\partial_3^2 E_1 + \partial_1 \partial_3 E_3) + \gamma_{33}(-\partial_1^2 E_3 + \partial_1 \partial_3 E_1). \end{aligned} \tag{21}$$

These are the equations to be solved in inhomogeneous media. Equations (21) reduce to (15) in homogeneous media. However, condition (7) has to be satisfied, whose implementation is shown in the following for the 3-D case.

Next, I impose condition (7) to the solution of Equations (5). The condition has the explicit form:

$$\begin{aligned} \partial_1(\sigma_{11}E_1 + \sigma_{12}E_2 + \sigma_{13}E_3) + \partial_2(\sigma_{12}E_1 + \sigma_{22}E_2 + \sigma_{23}E_3) \\ + \partial_3(\sigma_{13}E_1 + \sigma_{23}E_2 + \sigma_{33}E_3) = 0. \end{aligned} \tag{22}$$

It is enough to consider the  $y$ - and  $z$ -derivatives of  $\text{div } \mathbf{E}$ . From (22) we obtain

$$\begin{aligned} Y \equiv \partial_2 E_2 &\simeq -\sigma_{22}^{-1}[\partial_1(\sigma_{11}E_1) + \partial_3(\sigma_{33}E_3) + A], \\ Z \equiv \partial_3 E_3 &\simeq -\sigma_{33}^{-1}[\partial_1(\sigma_{11}E_1) + \partial_2(\sigma_{22}E_2) + A], \end{aligned} \tag{23}$$

where

$$A = \partial_1(\sigma_{12}E_2 + \sigma_{13}E_3) + \partial_2(\sigma_{12}E_1 + \sigma_{23}E_3) + \partial_3(\sigma_{13}E_1 + \sigma_{23}E_2), \tag{24}$$

and I have neglected derivatives of the diagonal conductivity components,  $\partial_i \sigma_{ii}$ , which yield unstable solutions. These derivatives involve terms of the form  $-E_i \partial_i \ln \sigma_{ii}$  (no implicit summation), which are numerically unstable due to the factor  $\sigma_{ii}^{-1} \partial_i \sigma_{ii}$ , where abrupt changes of the conductivity components occur. Further research is necessary to verify if the present algorithm can be used with an electric-magnetic formulation of Maxwell's equations, where derivatives of the material properties are avoided [9, 36]. A promising approach can be to solve a fictitious hyperbolic representation of the electromagnetic equations [20, 22].

The term  $\nabla \times \nabla \times \mathbf{E}$  appearing in Equation (5) is then computed as

$$\nabla \times \nabla \times \mathbf{E} = - \begin{pmatrix} (\partial_2^2 + \partial_3^2) E_1 - \partial_1(\partial_2 E_2 + Z) \\ (\partial_1^2 + \partial_3^2) E_2 - \partial_2(\partial_1 E_1 + Z) \\ (\partial_1^2 + \partial_2^2) E_3 - \partial_3(\partial_1 E_1 + Y) \end{pmatrix}. \quad (25)$$

In the isotropic and homogeneous case, the three components of the electric field decouple. Consider the first component of (25):  $\partial_1(\partial_2 E_2 + Z) = -\partial_1^2 E_1$ , since  $A = 0$ , and the conductivity is constant. Then, the spatial operator acting on  $E_1$  is  $-\nabla^2$ .

The algorithm for solving the differential equations is given in Appendix B, where the analysis for the anisotropic case is presented in detail. I use the regular Fourier method for computing the spatial derivatives along the horizontal direction and the Chebyshev differentiation [8] is used in the vertical direction to implement the air/ocean boundary condition (see Appendix C). The accuracy, stability and performance of the time-integration method based on the Chebyshev expansion is extensively analyzed in Tal-Ezer [30] and Carcione [7].

#### 4. SIMULATIONS

I consider the following source vector

$$\mathbf{J}_S = \nabla \times \mathbf{A}, \quad \mathbf{A} = h(f_1, f_2, f_3)^\top. \quad (26)$$

The spatial distribution is a Gaussian of the form:

$$f_i(\mathbf{x}) = \exp[-c_i(\mathbf{x} - \mathbf{x}_0)^2], \quad (27)$$

where  $c_i$  is a constant. The time history is a Ricker wavelet:

$$h(t) = \left(a - \frac{1}{2}\right) \exp(-a), \quad a = \left[\frac{\pi(t - t_s)}{t_p}\right]^2, \quad (28)$$

where  $t_p$  is the period of the wave (the distance between the side peaks is  $\sqrt{6}t_p/\pi$ ) and I take  $t_s = 1.4t_p$ . Its frequency spectrum is

$$H(\omega) = \left( \frac{t_p}{\sqrt{\pi}} \right) \bar{a} \exp(-\bar{a} - i\omega t_s), \quad \bar{a} = \left( \frac{\omega}{\omega_p} \right)^2, \quad \omega_p = \frac{2\pi}{t_p}. \quad (29)$$

The peak frequency is  $f_p = 1/t_p$ .

All the simulations assume a magnetic permeability  $\mu = \mu_0$ . First, I consider two cases in a 2-D isotropic space: i)  $\sigma = 0.5 \text{ S/m}$  (sediments) and  $f_p = 10 \text{ Hz}$ , and ii)  $\sigma = 3.6 \text{ S/m}$  (seawater) and

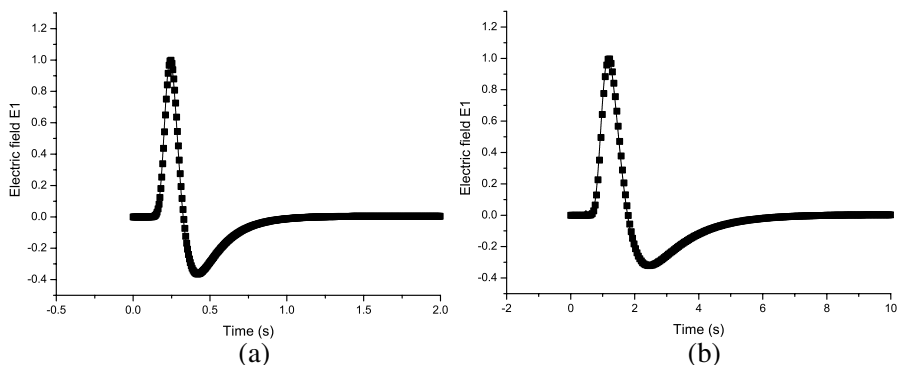


**Figure 1.** 2-D numerical simulation for cases i) (a) and ii) (b) (see text). Numerical and analytical electric field  $E_1$  at 2 km from the source (symbols and solid line, respectively).

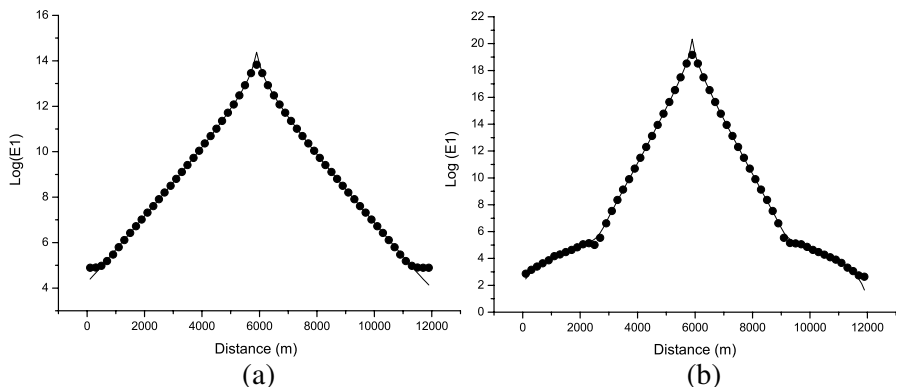


**Figure 2.** 2-D numerical simulation for cases i) (a) and ii) (b) (see text). Numerical and analytical AVO response (symbols and solid line, respectively). The frequency is 1 Hz.

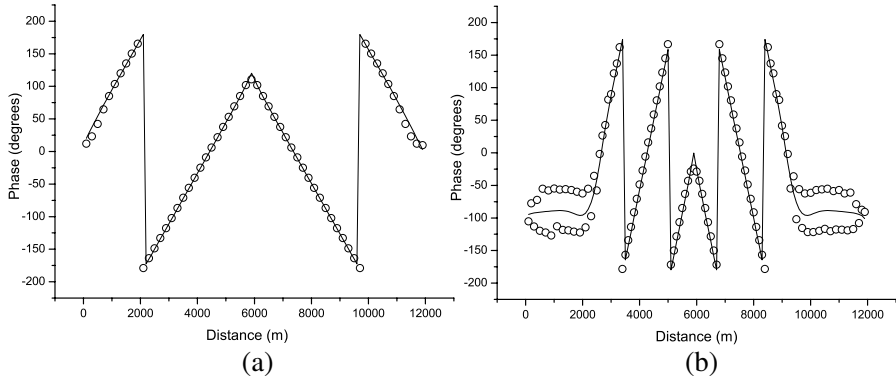


**Figure 3.** 2-D numerical simulation cases i) (a) and ii) (b) (see text). Numerical and analytical PVO response (symbols and solid line, respectively). The frequency is 1 Hz.

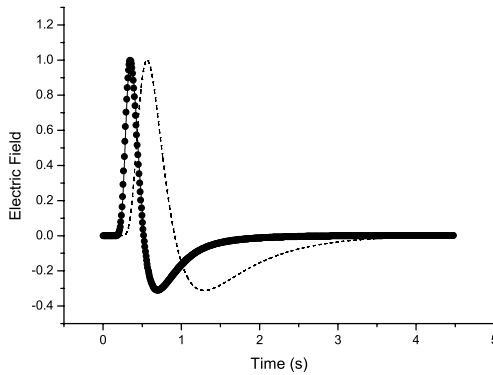


**Figure 4.** 2-D simulation for the anisotropic case. Numerical and analytical electric-field component  $E_1$  at 2 km from the source (symbols and lines, respectively). The dashed line corresponds to the isotropic case with  $\sigma_3 = \sigma_1 = 0.5$  S/m. The fields are normalized to 1, with the isotropic case weaker than the anisotropic case by a factor 5.

$f_p = 3$  Hz. From the first component of (13) ( $E = E_1$ ), and redefining the source term compared to (5), the equation to solve is

$$\frac{\partial E}{\partial t} = \frac{1}{\mu\sigma}(\partial_1^2 + \partial_3^2)E + J_S, \tag{30}$$

where  $J_S = \partial_3 f h(t)$ , and  $f$  has the form (27). One of the problems of using low-order finite differences for time stepping is that implementation of the source has to be performed by imposing initial

conditions [25], otherwise the source singularity generates noise in the solution. On the other hand, using the Chebyshev method I can use a source term as indicated in Appendix B (see, particularly, the section dealing with the source implementation). The sampling rate has to be smaller than  $1/(4f_p)$  if  $2f_p$  is taken as the maximum source frequency. The number of grid points is  $n_x = n_z = 119$  and the grid spacing is  $dx = dz = 100$  m. The source is located at the grid point (59, 59) and the receiver at (79, 59), i.e., 2 km from the source. The algorithm has  $b = 879$  1/s and  $M = 117$  (case i), and  $b = 407$  1/s and  $M = 80$  (case ii). The analytical solution is given by Equation (A10), with  $N = 2$ . Figures 1(a) and 1(b) compare the numerical and analytical solutions for cases i) and ii), respectively, where the symbols correspond to the simulations. The AVO (amplitude variations with offset) and PVO (phase variations with offset) responses at 1 Hz are given in Figures 2 and 3, respectively. The phase oscillates due to numerical noise at large offsets in case ii). Note that the amplitude of the field is 15 orders of magnitude less than the zero-offset field, due to the strong attenuation after 4 km propagation in seawater. The simulation must be performed to large enough times for the transients to decay sufficiently. The anomaly observed in Figure 2(b) beyond an offset of 2.5 km is due to this problem. In this case, the attenuation is very strong (seawater) and the decay is slower than in the case of the sediment (Figure 2(a)).

I consider now the 2-D anisotropic case for a homogeneous medium, described by Equation (16). Matrix  $\mathbf{G}$  involved in the formal solution (B8) is an scalar:  $G = \Delta_\gamma$ . Following the method outlined in Appendix B, the eigenvalues of  $G$  at the Nyquist wavenumber are

$$\kappa = -\frac{\pi^2}{dx^2}(\gamma_1 + \gamma_3) = -\frac{\pi^2}{\mu dx^2} \left( \frac{1}{\sigma_1} + \frac{1}{\sigma_3} \right), \quad (31)$$

where  $dz = dx$  has been assumed. The value of  $b$  to obtain convergence is  $|\kappa|$ . As an example I consider  $\sigma_1 = 0.5$  S/m,  $\sigma_3 = 0.25$  S/m, and  $f_p = 10$  Hz. The number of grid points and grid spacings are the same as the previous example. The source is located at the grid point (59, 59) and the receiver at (79, 59), i.e., at 2 km from the source. The algorithm has  $b = 1055$  1/s and  $M = 128$ . The analytical solution is given by Equation (A15). Figures 4 compares the numerical and analytical solutions, corresponding to the horizontal component  $E_1$  of the electric field, where the symbols correspond to the simulations. (The vertical component is zero.) The agreement is very good. The AVO and PVO responses at 3 Hz are given in Figure 5. The solid lines correspond to the anisotropic solution and the dashed lines to the isotropic solution. This is given by  $\sigma_{33} = \sigma_{11} = 0.5$  S/m. Important differences can be seen at all the offsets. If  $\sigma_{13} \neq 0$ , the

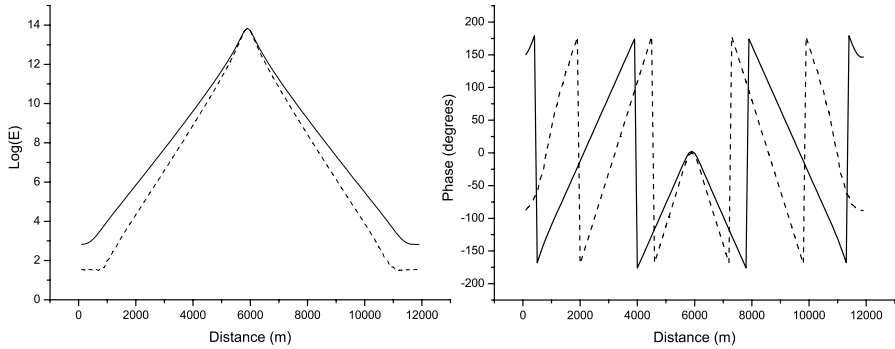


**Figure 5.** 2-D simulation for the anisotropic case. AVO and PVO responses (solid lines) compared to the isotropic case (dashed lines). The frequency is 3 Hz.

vertical component  $E_3$  is not zero, since  $E_1$  and  $E_3$  are coupled (see Equation (21)).

The next simulations considers a 3-D unbounded anisotropic medium, and I first test the algorithm against the analytical solution for an uniaxial medium (see Appendix A). I take  $\sigma_1 = \sigma_2 = 3.6$  S/m and  $\sigma_3 = 1.8$  S/m, and solve Equation (5) assuming the representation (25) for  $\nabla \times \nabla \times \mathbf{E}$ . The number of grid points is  $n_x = n_y = n_z = 119$  and the grid spacing is  $dx = dy = dz = 100$  m. The source has a central frequency  $f_p = 3$  Hz and is located at the grid point (59, 59, 59), while the receiver is placed at (79, 59, 59), i.e., 2 km from the source. The algorithm has  $b = 10171$ /s and  $M = 126$ . Figure 6 shows the comparison, where the RMS misfit error is  $1.2 \times 10^{-3}$ , i.e., the method is reasonably accurate due to the spectral nature of the algorithm.

Next, I consider the conductivity tensor

$$\boldsymbol{\sigma} = \begin{pmatrix} 3.6 & 1.08 & 0.72 \\ 1.08 & 3.6 & 0 \\ 0.72 & 0 & 1.8 \end{pmatrix}$$

in S/m. In this case, the source is defined by  $\mathbf{A} = h(0, 0, f_3)^\top$ , and the location of source and receiver is the same of the previous simulation. Figure 7 shows the three components of the electric field.

In the following, I compute the AVO and PVO curves for the model shown in Figure 8, where the medium below the seafloor is anisotropic. The number of grid points is  $n_x = 119$ ,  $n_y = 63$  and  $n_z = 67$ ; the grid spacing in the horizontal direction is  $dx = dy = 100$  m, while the vertical dimension is 4 km. The boundary condition (C3) is implemented at the air/ocean interface. The source is defined by

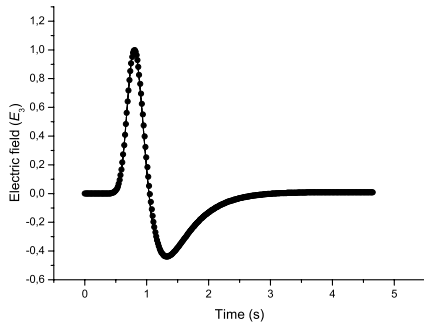


**Figure 6.** 3-D simulation for the anisotropic case. Numerical and analytical electric-field component  $E_3$  (symbols and solid line, respectively). The fields are normalized to 1.

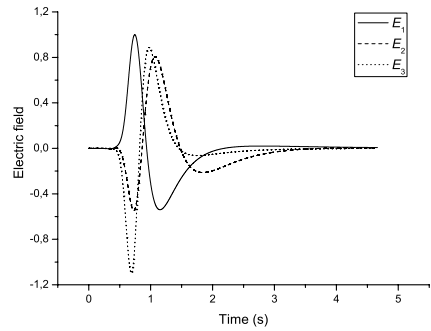


**Figure 7.** 3-D simulation for the anisotropic case. The plots shows the three components of the electric field, where the solid, dashed and dotted lines correspond to  $E_1$ ,  $E_2$  and  $E_3$ , respectively.

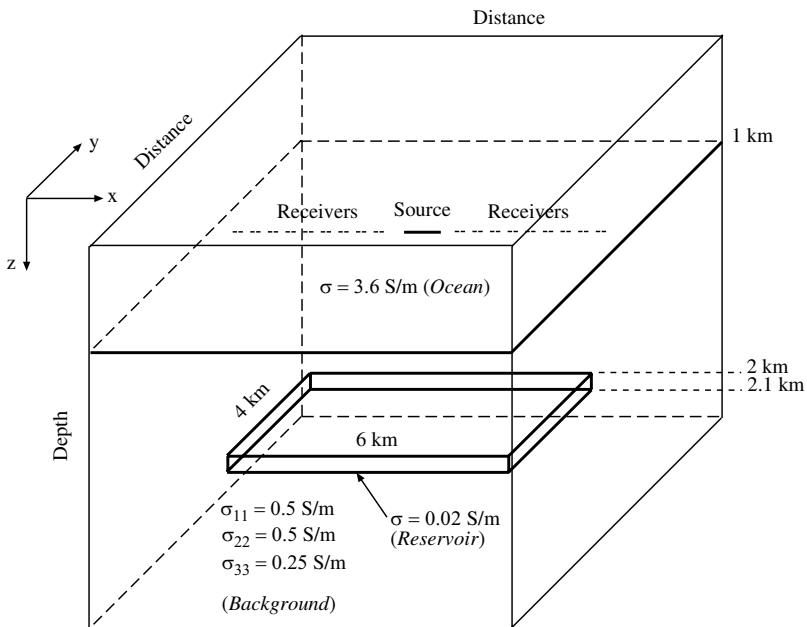


**Figure 8.** 3-D geological model.

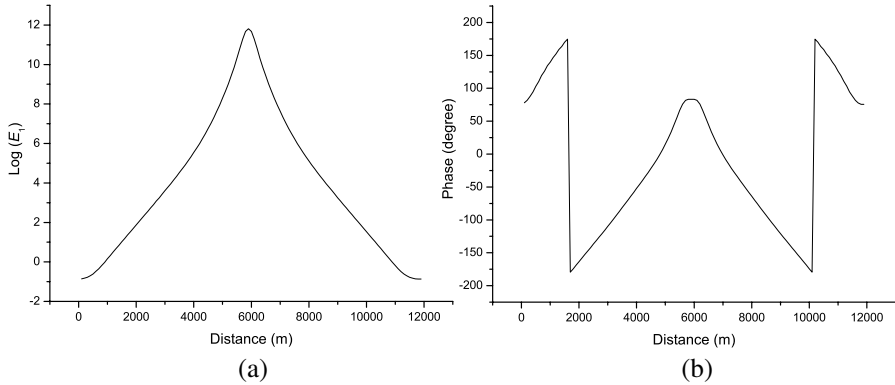


**Figure 9.** 3-D simulation corresponding to the model shown in Figure 7, where the AVO and PVO responses of the electric component  $E_1$  are shown. The frequency is 1 Hz.

$\mathbf{A} = h(0, f_2, 0)^\top$ , has a central frequency  $f_p = 10$  Hz and is located at the grid point (59, 31, 18). The receiver line is defined by the grid point  $(i, 31, 19)$ ,  $i = 1, \dots, n_x$  (the  $z$ -points 18 and 19 corresponds to the sea and the background, respectively). The algorithm computes the solution in one time step of 2.8 s, with  $b = 749376$  1/s and  $M = 5193$ . The AVO and PVO responses are shown in Figures 9(a) and 9(b), respectively.

## 5. CONCLUSIONS

I have developed a direct numerical method for modeling electromagnetic diffusion in an anisotropic earth, where the electric formulation is solved with a spectral Chebyshev expansion of the evolution operator. Pseudospectral methods are used to compute the spatial derivatives. An approximate version of the divergence of the current-density vector equal to zero is imposed to obtain the solution, which holds for inductively coupled sources.

The Chebyshev expansion, either for parabolic or hyperbolic problems, has spectral accuracy in time, and therefore avoids numerical dispersion, which is a characteristic feature of low-order schemes. The spatial derivatives computed with the Fourier pseudospectral method, which also has spectral accuracy and allows the use of coarser grids compared to FD methods. The modeling allows general material variability, a non-diagonal conductivity tensor and provides snapshots and time histories of the electric and magnetic fields. The use of this spectral method overcomes two drawbacks: low accuracy and stringent

stability conditions, since the error in time decays exponentially. Tests with Green's function solutions are successfully performed, showing that the RMS error is reasonably small.

The simulations focus on offshore applications, where it is necessary to model the air/ocean boundary condition and the diffusion at the ocean/sediment interface. The solution is given in the time domain and as amplitude and phase variations as a function of the source-receiver offset in the frequency domain.

This work offers an alternative algorithm to compute diffusion fields for practical applications. Further research is needed to avoid the approximation when implementing the divergence condition. This implies the use of the Chebyshev expansion with an electric-magnetic formulation of Maxwell's equations, where derivatives of the material properties can be avoided.

## APPENDIX A. ANALYTICAL SOLUTIONS

### A.1. 3-D Homogeneous Isotropic Medium

I derive a closed-form frequency-domain analytical solution for electromagnetic waves propagating in a 3-D unbounded homogeneous isotropic medium. If the source is divergence-free, it is  $\nabla \cdot \mathbf{E} = 0$  from  $\text{div} \cdot \mathbf{J} = 0$ . Then, Maxwell's Equation (13) for a time-harmonic field is

$$\nabla^2 \mathbf{E} - \omega \mu \sigma \mathbf{E} = \omega \mu \mathbf{J}_S, \quad (\text{A1})$$

where  $\omega$  is the angular frequency and  $\iota = \sqrt{-1}$ . Each component of the electric field satisfies

$$\nabla^2 E_i + \left(\frac{\omega}{v}\right)^2 E_i = \omega \mu J_{Si}, \quad i = 1, \dots, 3, \quad (\text{A2})$$

where

$$v = (1 + \iota) \sqrt{\frac{\omega}{2\mu\sigma}} \quad (\text{A3})$$

are complex velocities. As can be seen, each electric-field component is associated only with the conductivity component along the same direction. This is the TE mode on the Cartesian planes.

Consider the Green's function solution for each Equation (A2) and denote each field component by  $E$ . It is

$$\nabla^2 g + \left(\frac{\omega}{v}\right)^2 g = -\delta(x)\delta(y)\delta(z). \quad (\text{A4})$$

where [8]

$$g(r) = \frac{1}{4\pi r} \exp(-\iota kr), \quad k = \frac{\omega}{v}, \quad (\text{A5})$$

with

$$r = \sqrt{x^2 + y^2 + z^2}. \quad (\text{A6})$$

If I assume a source of the form:

$$J_S = -J_0 \mu^{-1} \delta(x) \delta(y) \delta(z) H(\omega), \quad (\text{A7})$$

where  $H$  is the Fourier transform of the time history  $h$ , the solution for the electric components is

$$E(r, \omega) = i\omega J_0 H(\omega) g(r, \omega), \quad (\text{A8})$$

or

$$E(r, t) = J_0 \partial_t h * g. \quad (\text{A9})$$

where “\*” denotes time convolution. To ensure a real time-domain solution, I consider an Hermitian frequency-domain solution, and the time-domain solution is obtained from (A8) by an inverse transform.

Actually, Equation (A9) and (A10) holds for a complex conductivity, i.e., including induced polarization effects [39]. If the conductivity is real and  $h(t)$  is the Heaviside function, Equation (A10) has the following solution solution

$$E(r, t) = \frac{J_0}{(4\pi t)^{N/2}} \exp[-\mu\sigma r^2/(4t)], \quad (\text{A10})$$

where  $N$  is the dimension of the space [10].

## A.2. 2-D Homogeneous Anisotropic Medium

Consider one of the Equations (16), denoting  $E_1$  or  $E_3$  by  $E$ . Redefining the source term, I have

$$\Delta_\gamma E - \partial_t E = J_S, \quad \Delta_\gamma = \gamma_1 \partial_3^2 + \gamma_3 \partial_1^2 = \frac{1}{\mu\sigma_3} \partial_1^2 + \frac{1}{\mu\sigma_1} \partial_3^2. \quad (\text{A11})$$

Defining  $x' = x/\sqrt{\gamma_3}$  and  $z' = z/\sqrt{\gamma_1}$ , I obtain

$$\Delta' E - \partial_t E = J_S, \quad \Delta' = \frac{\partial^2}{\partial x'^2} + \frac{\partial^2}{\partial z'^2}. \quad (\text{A12})$$

The solution for the Green function is obtained for  $J_S = -\delta(x', z')\delta(t)$ . I get [10]

$$g(x, z, t) = \frac{1}{4\pi t} \exp[-r'^2/(4t)], \quad (\text{A13})$$

where

$$r' = \sqrt{x'^2 + z'^2} = \sqrt{\frac{x^2}{\gamma_1} + \frac{z^2}{\gamma_3}} = \sqrt{\mu} \sqrt{\sigma_3 x^2 + \sigma_1 z^2} \quad (\text{A14})$$

If  $J_S = -\delta(x, z)h(t)$ , the solution is given by

$$E = g * h. \quad (\text{A15})$$

### A.3. 3-D Homogeneous Transversely Isotropic (Uniaxial) Medium

A 3-D analytical solution for the  $E_3$ -component, based on equation (18), can be obtained by using the same coordinate transformation of the previous section. In this case,

$$\Delta_\gamma E_3 - \partial_t E_3 = J_S, \quad \Delta_\gamma = \frac{1}{\mu\sigma_3}(\partial_1^2 + \partial_2^2) + \frac{1}{\mu\sigma_1}\partial_3^2. \quad (\text{A16})$$

Defining  $x' = x/\sqrt{\gamma_3}$ ,  $y' = y/\sqrt{\gamma_3}$  and  $z' = z/\sqrt{\gamma_1}$ , I obtain

$$\Delta' E_3 - \partial_t E_3 = J_S, \quad \Delta' = \frac{\partial^2}{\partial x'^2} + \frac{\partial^2}{\partial y'^2} + \frac{\partial^2}{\partial z'^2}. \quad (\text{A17})$$

The solution for the Green function is obtained for  $J_S = -\delta(x', y', z')\delta(t)$ . I get [10]

$$g(x, y, z, t) = \frac{1}{(4\pi t)^{3/2}} \exp[-r'^2/(4t)] \quad (\text{A18})$$

where

$$r' = \sqrt{\mu} \sqrt{\sigma_3(x^2 + y^2) + \sigma_1 z^2} \quad (\text{A19})$$

If  $J_S = -\delta(x, y, z)h(t)$ , the solution is given by

$$E_3 = g * h. \quad (\text{A20})$$

## APPENDIX B. TIME INTEGRATION

The electric formulation is solved with the spectral Chebyshev method [7]. First, I illustrate the simplest FD time-domain algorithm to solve Equation (13) (homogeneous case). Assume for simplicity the following representation for each component:

$$\partial_t E = \frac{1}{\mu\sigma} \Delta E + J_S \quad (\text{B1})$$

where  $\Delta$  is the Laplacian. The problem can be solved with the forward Euler technique:

$$E^{n+1} = E^n + \frac{dt}{\mu\sigma} \Delta E^n + dt J_S^n, \quad (\text{B2})$$

or the staggered scheme

$$E^{n+1/2} = E^{n-1/2} + \frac{dt}{\mu\sigma} \Delta E^n + dt J_S^n. \quad (\text{B3})$$

Assume a plane-wave solution  $E^n = \exp(\omega ndt - ikx)$ . The last equation without sources can be written as

$$2i \sin\left(\frac{\omega dt}{2}\right) = -\frac{dk^2}{\mu\sigma}. \quad (\text{B4})$$

Since the absolute value of the sine function has to be less or equal to one, I obtain the stability condition:

$$dt \leq \frac{2\mu\sigma dx^2}{3\pi^2}, \quad (\text{B5})$$

where  $dx$  is the minimum grid size, and I have considered the Nyquist spatial wavenumber  $k = \sqrt{3}\pi/dx$  (the factor 3 holds for the 3-D space, since  $k^2 = k_1^2 + k_2^2 + k_3^2$ , where  $k_i$  are the wavenumber components). Another way to find this condition is to assume a solution  $E^n = G \exp(-ikx)$ , where  $G$  is the growth factor. I obtain from Equation (B2):

$$E^{n+1} = GE^n, \quad G = 1 - dt(\mu\sigma)^{-1}k^2. \quad (\text{B6})$$

Stability requires  $|G| \leq 1$  (this is equivalent to the von Neumann stability condition, discussed in the previous section). Again, the worst case is when the wavenumber is the Nyquist one. That condition gives  $dt(\mu\sigma)^{-1}k^2 \leq 2$  and therefore Equation (B5).

The Chebyshev method to solve Equation (5) (inhomogeneous case) is discussed in the following. I re-write that equation as

$$\partial_t \mathbf{E} = \mathbf{G} \mathbf{E} + \mathbf{s}, \quad \mathbf{G} = -(\mu\sigma)^{-1} \cdot \nabla \times \nabla \times, \quad (\text{B7})$$

where  $\mathbf{s}$  is the source term and  $\mu$  is assumed to be constant. Considering a discretization with  $N$  grid points, the system (13) becomes a coupled system of  $L \cdot N$  ordinary differential equations at the grid points, where  $L$  is the dimension of matrix  $\mathbf{G}$ . The solution to Equation (B7) subject to the initial condition  $\mathbf{E}(0) = \mathbf{E}_0$  is formally given by

$$\mathbf{E}_N(t) = \exp(t\mathbf{G}_N)\mathbf{E}_N^0 + \int_0^t \exp(\tau\mathbf{G}_N)\mathbf{s}_N(t - \tau)d\tau, \quad (\text{B8})$$

where  $\mathbf{E}_N^0$  is the initial-condition field vector,  $\exp(t\mathbf{G}_N)$  is called the evolution operator, and the subscript  $N$  indicates that those quantities are discrete representation of the respective continuous quantities. I consider a separable source term  $\mathbf{s}_N = \mathbf{a}_N h(t)$ , where  $\mathbf{a}_N$  is the spatial distribution of the source and the function  $h(t)$  is the source time history. A discrete solution of (B8) is achieved by approximating the evolution operator. For instance, in the absence of a source, the solution can be expressed by

$$\mathbf{E}_N(t) = H_M(t\mathbf{G}_N)\mathbf{E}_N^0, \quad (\text{B9})$$

where  $H_M$  is a polynomial of degree  $M$  that converges to  $\exp(t\mathbf{G}_N)$  in the domain that includes all the eigenvalues of the operator  $t\mathbf{G}_N$ . I use the following Chebyshev expansion of  $\exp(u)$  [1, 30]:

$$\exp(u) = \sum_{k=0}^{\infty} \alpha_k(bt)T_k\left(\frac{u}{bt}\right), \tag{B10}$$

where  $\alpha_k$  are the expansion coefficients,  $T_k$  is the Chebyshev polynomial of order  $k$ , and  $b$  is the absolute value of the eigenvalue of matrix  $\mathbf{G}_N$  having the largest negative real part (as we shall see later, the eigenvalues of the electric formulation are located on the real axis and their real part is negative). For convergence,  $|u| \leq bt$  and  $u$  lies on the real axis. The expansion coefficients are given by

$$\alpha_k = c_k I_k, \quad c_0 = 1, \quad c_k = 2, \quad k \geq 1, \tag{B11}$$

and  $I_k$  is the modified Bessel function of order  $k$ .

I perform the change of variable

$$w = \frac{1}{bt}(u + bt), \quad -1 \leq w \leq 1. \tag{B12}$$

From Equations (B10) and (B12),

$$\exp(u) = \exp(-bt) \exp(btw) = \sum_{k=0}^{\infty} \beta_k T_k(w), \tag{B13}$$

where

$$\beta_k = \alpha_k \exp(-bt) = c_k \exp(-bt) I_k(bt) \tag{B14}$$

for initial conditions without source, and

$$\beta_k = c_k \int_0^t \exp(-b\tau) I_k(b\tau) h(t - \tau) d\tau \tag{B15}$$

in the presence of a source (without initial conditions). The reason for the change of variable  $u$  to  $w$  is to avoid the calculation of Bessel functions when the argument  $bt$  is large, since this may exceed the dynamic range of the computer. Instead, the quantity  $\exp(-bt)I_k(bt)$  is computed.

For computations, the expansion (B13) has to be truncated. Thus, the  $M$  degree polynomial approximation of  $\exp(x)$  is

$$H_M(u) = \sum_{k=0}^M \beta_k T_k(w(u)). \tag{B16}$$

Because  $u$  in (B10) is replaced by  $t\mathbf{G}_N$ , the variable  $w$  defined in Equation (B12) is represented by an operator  $\mathbf{F}_N$  defined as

$$\mathbf{F}_N = \frac{1}{b}(\mathbf{G}_N + b\mathbf{I}), \tag{B17}$$

where  $\mathbf{I}$  is the identity matrix of dimension  $L$ . In the absence of sources, the discrete solution is

$$\mathbf{E}_N^M(t) = \sum_{k=0}^M \beta_k(t) T_k(\mathbf{F}_N) \mathbf{E}_N^0. \quad (\text{B18})$$

$T_k(\mathbf{F}_N) \mathbf{E}_N^0$  is computed by using the recurrence relation of the Chebyshev polynomials [1],

$$T_k(w) = 2wT_{k-1}(w) - T_{k-2}(w), \quad k \geq 2, \quad (\text{B19})$$

$$T_0(w) = 1, \quad T_1(w) = w \quad (\text{B20})$$

[1]. Hence,

$$T_k(\mathbf{F}_N) \mathbf{E}_N^0 = 2\mathbf{F}_N T_{k-1}(\mathbf{F}_N) \mathbf{E}_N^0 - T_{k-2}(\mathbf{F}_N) \mathbf{E}_N^0, \quad k \geq 2, \quad (\text{B21})$$

$$T_0(\mathbf{F}_N) \mathbf{E}_N^0 = \mathbf{E}_N^0, \quad T_1(\mathbf{F}_N) \mathbf{E}_N^0 = \mathbf{F}_N \mathbf{E}_N^0. \quad (\text{B22})$$

The algorithm is a three-level scheme, since it uses the recurrence relation. The first time step should be larger than the duration of the source. Results at small time steps to compute time histories at specified points of the grid do not require significant computational effort. A slight modification of Equation (B18) can be used:

$$\mathbf{E}_N^M(t') = \sum_{k=0}^M \beta_k(t') T_k(\mathbf{F}_N) \mathbf{E}_N^0, \quad (\text{B23})$$

for  $t < t'$ . This calculation does not require significantly more computations since the terms involving the spatial derivatives  $T_k(\mathbf{F}_N) \mathbf{E}_N^0$  do not depend on the time variable and are calculated in any case. Only the coefficients  $\beta_k$  are time dependent, such that additional sets of Bessel functions need to be computed.

The present algorithm has infinite accuracy in time and in space, and is highly efficient, since the stability condition requires a time step  $dt = O(1/N)$  compared to  $dt = O(1/N^2)$  for finite-order explicit schemes. Moreover, the error in time decays exponentially [30].

### B.0.1. Eigenvalues of the Propagation Matrix

In the Fourier domain, the time derivative is replaced by  $i\omega$ , where  $\omega$  is the angular frequency, and the spatial derivatives  $\partial_i$  are replaced by  $ik_i$ , where  $k_i$  are the components of the wavenumber vector. Replacing the wavenumber components into Equation (B7) and assuming constant material properties, I obtain

$$\mathbf{G} = \begin{pmatrix} -(k_2^2 + k_3^2)a_1^{-1} & k_1k_2a_1^{-1} & k_1k_3a_1^{-1} \\ k_1k_2a_2^{-1} & -(k_1^2 + k_3^2)a_2^{-1} & k_2k_3a_2^{-1} \\ k_1k_3a_3^{-1} & k_2k_3a_3^{-1} & -(k_1^2 + k_2^2)a_3^{-1} \end{pmatrix}, \quad (\text{B24})$$

whose eigenvalues are 0, and

$$g_{\pm} = -\frac{1}{2}(A \pm \sqrt{B}), \tag{B25}$$

where

$$\begin{aligned} A &= k_1^2 b_1 + k_2^2 b_2 + k_3^2 b_3, \\ B &= -4k^2(a_2 a_3 k_1^2 + a_1 a_3 k_2^2 + a_1 a_2 k_3^2) \\ &\quad + [a_3(k_1^2 + k_2^2) + a_2(k_1^2 + k_3^2) + a_1(k_2^2 + k_3^2)]^2, \\ k^2 &= k_1^2 + k_2^2 + k_3^2, \\ b_i &= a_j + a_k, \quad i \neq j \neq k, \\ a_i &= (\mu\sigma_i)^{-1}. \end{aligned} \tag{B26}$$

It can be shown that these eigenvalues are real and negative. In the isotropic case,  $B = 0$  and the eigenvalues are 0 and  $-k^2(\mu\sigma)^{-1}$  with multiplicity two.

The maximum wavenumber components are the Nyquist wavenumbers, which for grid spacings  $dx_i$  are  $k_i = \pi/dx_i$ . They are related to the highest harmonics of the spatial Fourier transform. Hence, the value of  $b$  is obtained by replacing the Nyquist wavenumbers in Equation (B25) and taking the eigenvalue with maximum absolute value, i.e.,

$$b = \max(|g_+|, |g_-|) = |g_+|. \tag{B27}$$

If  $dx = dy = dz$ , I obtain

$$b = \frac{\pi^2}{dx^2} \left( a_1 + a_2 + a_3 + \sqrt{a_1^2 + a_2^2 + a_3^2 - a_1 a_2 - a_1 a_3 - a_2 a_3} \right). \tag{B28}$$

In the isotropic case, I have

$$b = \frac{3}{\mu\sigma} \left( \frac{\pi}{dx} \right)^2. \tag{B29}$$

Alternatively, the single eigenvalue of matrix  $\mathbf{G}$  associated with Equation (13) can easily be obtained as

$$g_i = -\frac{1}{\mu\sigma_i} (k_1^2 + k_2^2 + k_3^2), \tag{B30}$$

and  $b$  is given by an equation similar to (B29) for the Nyquist wavenumbers and cubic cells. Note that  $dt \leq 2/b$ , where  $dt$  is the FD time step (B5).

As Tal-Ezer [30] has shown, the polynomial order should be  $O(\sqrt{bt})$  (his Equation (4.13)). I found that

$$M = K\sqrt{bt} \tag{B31}$$

is enough to obtain stability and accuracy, where  $K$  ranges from 4 to 6. On the other hand, a safe value of  $M$  can be determined by finding the range in which the coefficients  $\beta_k$  are significantly different from zero (for instance, by checking the ratio  $\beta_0/\beta_m$ ).

### B.1. Source Implementation

The implementation of a single-point source generates a strong high-frequency image of the initial source time history at earlier propagation times. This noise is common in pseudospectral methods. This event is attenuated by using the Gaussian spatial distribution for the source along the source-receiver direction. Seven grid points are enough, with the amplitudes defined by  $\exp[-0.5(i - i_0)^2]$ , where  $i_0$  is the relative source location (in grid points) corresponding to  $i = 4$ .

Moreover, the source central frequency has to be as low as possible. Note that a lower dominant frequency implies a longer source duration and therefore a longer first time step of the algorithm, which increases the argument of the Bessel functions  $bt$  (see Equation (B15)). This makes the introduction of the source more expensive. On the other hand,  $b$  decreases with increasing conductivity (see Equation (B29)), thus reducing the computer time.

An alternative approach is to solve for secondary fields, to avoid the problem of the source singularity. The equations can be reformulated in terms of the secondary field  $\mathbf{E}^s$ , defined as the difference between the total field  $\mathbf{E}^s$  and the primary field of a background model  $\mathbf{E}^p$ , i.e.,  $\mathbf{E} = \mathbf{E}^p + \mathbf{E}^s$ . The source term then becomes  $\mu(\boldsymbol{\sigma} - \boldsymbol{\sigma}_0) \cdot \partial_t \mathbf{E}^p$ , where  $\boldsymbol{\sigma}_0$  is the background conductivity [2].

## APPENDIX C. AIR/WATER BOUNDARY CONDITION

The air, assumed homogeneous, obeys Equation (13). Since the conductivity vanishes, I obtain the Laplace equation

$$\nabla^2 \mathbf{E} = 0. \quad (\text{C1})$$

In the 2-D case when only one component of the electric field is computed (the TE mode, perpendicular to the plane of propagation), I use the approach of Oristaglio and Hohmann [25]. I compute the vertical spatial derivative using the Chebyshev spectral method [8] and assume that the grid points of the first row are in the air. Then, the field here is obtained as

$$E(k_1, z = -d) = \frac{1}{2\pi} \int_{-\infty}^{\infty} \exp(|k_1|d + \imath k_1 x) E(k_1, z = 0) dk_1, \quad (\text{C2})$$

where  $E(k_1, z = 0)$  is the Fourier transform of the electric field at the air/water interface, and  $d$  is the grid spacing between the surface and the points in the air.

To apply the boundary condition in 3-D, I use the upward-continuation scheme of Wang and Hohmann [32] to compute  $E_1$  and  $E_2$  above the surface using  $E_3$  on the surface:

$$E_1(k_1, k_2, z = -d) = -\frac{ik_1 \exp\left(-d\sqrt{k_1^2 + k_2^2}\right)}{\sqrt{k_1^2 + k_2^2}} E_3(k_1, k_2, z = 0), \quad (\text{C3})$$

$$E_2(k_1, k_2, z = -d) = \frac{k_2}{k_1} E_1(k_1, k_2, z = -d),$$

where  $d$  is the grid spacing between the surface and the points in the air. The method consists of transforming  $E_3$  to the  $(k_1, k_2)$ -domain, use of Equations (C3) and inverse Fourier transforms to obtain the horizontal components in the air.

In the 2-D anisotropic case, Equation (C3) becomes

$$E_1(k_1, z = -d) = -i \exp(-dk_1) E_3(k_1, z = 0). \quad (\text{C4})$$

## REFERENCES

1. Abramowitz, M., and I. A. Stegun, *Handbook of mathematical functions*, Dover, 1972.
2. Adhidjaja, J. I., G. W. Hohmann, and M. L. Oristaglio, "Two-dimensional transient electromagnetic responses," *Geophysics*, Vol. 50, 2849–2861, 1985.
3. Al-Garni, M. and M. E. Everett, "The paradox of anisotropy in electromagnetic loop-loop responses over a uniaxial half-space," *Geophysics*, Vol. 68, 892–899, 2003.
4. Anderson, B., T. Barber, and S. Gianzero, "The effect of crossbedding anisotropy on induction tool response," *Petrophysics*, Vol. 42, 137–149, 2001.
5. Badea, E. A., M. E. Everett, G. A. Newman, and O. Biro, "Finite-element analysis of controlled-source electromagnetic induction using Coulomb-gauged potentials," *Geophysics*, Vol. 66, 786–799, 2001.
6. Carcione, J. M., "Ground penetrating radar: wave theory and numerical simulation in conducting anisotropic media," *Geophysics*, Vol. 61, 1664–1677, 1996.
7. Carcione, J. M., "A spectral numerical method for electromagnetic diffusion," *Geophysics*, Vol. 71, I1–I9, 2006.

8. Carcione, J. M., *Wave Fields in Real Media. Theory and Numerical Simulation of Wave Propagation in Anisotropic, Anelastic, Porous and Electromagnetic Media*, 2nd Edition, Elsevier, 2007.
9. Carcione, J. M. and M. Schoenberg, "3-D ground-penetrating radar simulation and plane wave theory," *Geophysics*, Vol. 65, 1527–1541, 2000.
10. Carslaw, H. S. and J. C. Jaeger, *Conduction of Heat in Solids*, Clarendon Press, 1984.
11. Davydycheva, S., V. Druskin, and T. Habashy, "An efficient finite-difference scheme for electromagnetic logging in 3D anisotropic inhomogeneous media," *Geophysics*, Vol. 68, 1525–1536, 2003.
12. Druskin, V. L. and L. A. Knizhnerman, "Spectral approach to solving three-dimensional Maxwells diffusion equations in the time and frequency domains," *Radio Science*, Vol. 29, 937–953, 1994.
13. Druskin, V. L., L. A. Knizhnerman, and P. Lee, "New spectral Lanczos decomposition method for induction modeling in arbitrary 3-D geometry," *Geophysics*, Vol. 64, 701–706, 1999.
14. Eidesmo, T., S. Ellingsrud, L. M. MacGregor, S. Constable, M. C. Sinha, S. Johansen, F. N. Kong, and H. Westerdahl, "Sea bed logging (SBL), a new method for remote and direct identification of hydrocarbon filled layers in deepwaters areas," *First Break*, Vol. 20, 144–151, 2002.
15. Everett, M. E. and S. Constable, "Electric dipole fields over an anisotropic seafloor: Theory and application to the structure of 40 Ma Pacific Ocean lithosphere," *Geophys. J. Int.*, Vol. 136, 41–56, 1999.
16. Jiang, B.-N., J. Wu, and L. A. Povinelli, "The origin of spurious solutions in computational electromagnetics," *Journal of Computational Physics*, Vol. 125, 104–123, 1996.
17. Kong, F. N., S. E. Johnstad, T. Røsten, and H. Westerdahl, "A 2.5D finite-element-modeling difference method for marine CSEM modeling in stratified anisotropic media," *Geophysics*, Vol. 73, F9–F19, 2008.
18. Lee, K. H., G. Liu, and H. F. Morrison, "A new approach to modeling the electromagnetic response of conductive media," *Geophysics*, Vol. 54, 1180–1192, 1989.
19. Leppin, M., "Electromagnetic modeling of 3-D sources over 2-D inhomogeneities in the time domain," *Geophysics*, Vol. 57, 994–1003, 1992.
20. Maaø, F., "Fast finite-difference time-domain modeling for

- marine-subsurface electromagnetic problems,” *Geophysics*, Vol. 72, A19–A23, 2007.
21. Mackie, R. L., T. R. Madden, and P. E. Wannamaker, “Three-dimensional magnetotelluric modeling using finite difference equations — Theory and comparisons to integral equation solutions,” *Geophysics*, Vol. 58, 215–226, 1993.
  22. Mittet, R., “High-order finite-difference simulations of marine CSEM surveys using a correspondence principle for wave and diffusion fields,” *Geophysics*, Vol. 75, F33–F50, 2010.
  23. Negi, J. G. and P. D. Saraf, *Anisotropy in Geoelectromagnetism*, Elsevier, New York, 1989.
  24. Olhoeft, G. R. and D. E. Capron, “Petrophysical causes of electromagnetic dispersion,” *Proceedings of the Fifth Internat. Conf. on Ground Penetrating Radar*, 145–152, University of Waterloo, 1994.
  25. Oristaglio, M. L. and G. W. Hohmann, “Diffusion of electromagnetic fields into a two-dimensional earth: A finite-difference approach,” *Geophysics*, Vol. 49, 870–894, 1984.
  26. Pellerin, L., J. M. Johnston, and G. W. Hohmann, “A numerical evaluation of electromagnetic methods in geothermal exploration,” *Geophysics*, Vol. 61, 121–130, 1996.
  27. Sasaki, Y. and M. A. Meju, “Useful characteristics of shallow and deep marine CSEM responses inferred from 3D finite-difference modeling,” *Geophysics*, Vol. 74, F67–F76, 2009.
  28. Smith, J. T., “Conservative modeling of 3-D electromagnetic fields: Part 2 — Biconjugate gradient solution and an accelerator,” *Geophysics*, Vol. 61, 1319–1324, 1996.
  29. Stalnaker, J. L., “A finite element approach to the 3D CSEM modeling problem and applications to the study of the effect of target interaction and topography,” PHD Thesis, Texas A&M University, 2004.
  30. Tal-Ezer, H., “Spectral methods in time for parabolic problems,” *SIAM Journal of Numerical Analysis*, Vol. 26, 1–11, 1989.
  31. Wang, T. and S. Fang, “3D electromagnetic anisotropy modeling using finite differences,” *Geophysics*, Vol. 66, 1386–1398, 2001.
  32. Wang, T. and G. W. Hohmann, “A finite-difference, time-domain solution for three-dimensional electromagnetic modeling,” *Geophysics*, Vol. 58, 797–809, 1993.
  33. Wang, T. and J. Signorelli, “Finite-difference modeling of electromagnetic tool response for logging while drilling,” *Geophysics*, Vol. 69, 152–160, 2004.

34. Weiss, C. J. and S. Constable, "Mapping thin resistors and hydrocarbons with marine EM methods, Part II — Modeling and analysis in 3D," *Geophysics*, Vol. 71, G321–G332, 2006.
35. Weiss, C. J. and G. A. Newman, "Electromagnetic induction in a fully 3D anisotropic earth," *Geophysics*, Vol. 67, 1104–1114, 2002.
36. Yee, K. S., "Numerical solution of initial boundary value problems involving Maxwells equations in isotropic media," *IEEE Transactions on Antennas and Propagation*, Vol. 14, 302–307, 1966.
37. Yin, C. and H. M. Maurer, "Electromagnetic induction in a layered earth with arbitrary anisotropy," *Geophysics*, Vol. 66, 1405–1416, 2001.
38. Yu, L., R. L. Evans, and R. N. Edwards, "Transient electromagnetic responses in seafloor with triaxial anisotropy," *Geophys. J. Int.*, Vol. 129, 292–304, 1997.
39. Zhdanov, M., "Generalized effective-medium theory of induced polarization," *Geophysics*, Vol. 73, F197–F211, 2008.